A conserved energetic footprint underpins recognition of human leukocyte antigen-E by two distinct αβ T cell receptors

Received for publication, July 20, 2017, and in revised form, September 20, 2017 Published, Papers in Press, September 25, 2017, DOI 10.1074/jbc.M117.807719

Lucy C. Sullivan[‡1,2], Nicholas G. Walpole[§1], Carine Farenc[§], Gabriella Pietra[¶‖], Matthew J. W. Sum[‡], Craig S. Clements[§], Eleanor J. Lee[‡], Travis Beddoe[§3], Michela Falco[**], Maria Cristina Mingari[¶‖‡‡], Lorenzo Moretta[**], Stephanie Gras[§ §§4], Jamie Rossjohn[§ §§¶¶5,6], and Andrew G. Brooks[‡5,7]

*From the [‡]Department of Microbiology and Immunology and Peter Doherty Institute for Infection and Immunity, University of Melbourne, Melbourne 3000, Australia, [§]Infection and Immunity Program and Department of Biochemistry and Molecular Biology, Biomedicine Discovery Institute and [§§]Australian Research Council Centre of Excellence in Advanced Molecular Imaging, Monash University, Clayton, Victoria 3800, Australia, [¶]Department of Experimental Medicine (DiMES) and [‡‡]Center of Excellence for Biomedical Research, University of Genoa, 16132 Genoa, Italy, [‖]Unità Operativa Complessa Immunologia, Ospedale Policlinico San Martino, 16132 Genoa, Italy, **Istituto di Ricovero e Cura a Carattere Scientifico Ospedale Pediatrico Bambino Gesù, 00165 Roma, Italy, and [¶¶]Institute of Infection and Immunity, Cardiff University School of Medicine, Heath Park, Cardiff CF14 4XN, Wales, United Kingdom*

Edited by Peter Cresswell

αβ T cell receptors (TCRs) interact with peptides bound to the polymorphic major histocompatibility complex class Ia (MHC-Ia) and class II (MHC-II) molecules as well as the essentially monomorphic MHC class Ib (MHC-Ib) molecules. Although there is a large amount of information on how TCRs engage with MHC-Ia and MHC-II, our understanding of TCR/MHC-Ib interactions is very limited. Infection with cytomegalovirus (CMV) can elicit a CD8$^+$ T cell response restricted by the human MHC-Ib molecule human leukocyte antigen (HLA)-E and specific for an epitope from UL40 (VMAPRTLIL), which is characterized by biased TRBV14 gene usage. Here we describe an HLA-E–restricted CD8$^+$ T cell able to recognize an allotypic variant of the UL40 peptide with a modification at position 8 (P8) of the peptide (VMAPRTLVL) that uses the TRBV9 gene segment. We report the structures of a TRBV9$^+$ TCR in complex with the HLA-E molecule presenting the two peptides. Our data revealed that the TRBV9$^+$ TCR adopts a different docking mode and molecular footprint atop HLA-E when compared with the TRBV14$^+$ TCR–HLA-E ternary complex. Additionally, despite their differing V gene segment usage and different docking mechanisms, mutational analyses showed that the TCRs shared a conserved energetic footprint on the HLA-E molecule, focused around the peptide-binding groove. Hence, we provide new insights into how monomorphic MHC molecules interact with T cells.

Major histocompatibility complex class I (MHC-I) molecules perform critical roles in regulating innate and adaptive immune responses. These molecules have evolved to bind both self- and pathogen-derived peptides and present them for recognition by diverse populations of cells, prominently cytotoxic T cells and natural killer (NK)[8] cells (1). There are two main classes of MHC-I molecules: classical MHC-I (MHC-Ia) molecules that constitute the major ligands for CD8$^+$ or cytotoxic T cells and non-classical MHC-I (MHC-Ib) molecules whose functions are less understood but, like their classical counterparts, are recognized by both the adaptive and innate immune systems (2).

The genes encoding MHC-Ia proteins are highly polymorphic with the polymorphisms being primarily clustered around six pockets located within the antigen-binding cleft. As peptide binding to MHC-Ia proteins is dependent on the accommodation of peptide side chains in these pockets, variation therein creates allotype-specific peptide binding properties (3). In contrast, MHC-Ib genes are far less polymorphic and in some cases, such as human leukocyte antigen (HLA)-E, essentially dimorphic (4). This restricted polymorphism may be associated with the additional distinct functions aside from the presentation of peptides to cytotoxic T cells. Nevertheless, the only identified function of many MHC-Ib molecules is the presentation of peptides for T cell recognition or the regulation of NK cell activity.

The authors declare that they have no conflicts of interest with the contents of this article.

The atomic coordinates and structure factors (codes 5W1W and 5W1V) have been deposited in the Protein Data Bank (http://wwpdb.org/).

[1] Joint first authors.

[2] Supported by a National Health and Medical Research Council career development award.

[3] Present address: Dept. of Animal, Plant and Soil Science and Centre for AgriBioscience (AgriBio), La Trobe University, Melbourne, Victoria 3086, Australia.

[4] Supported by a Monash senior research fellowship.

[5] Joint senior authors.

[6] Supported by an Australian Research Council laureate fellowship. To whom correspondence may be addressed. E-mail: jamie.rossjohn@monash.edu.

[7] To whom correspondence may be addressed. E-mail: agbrooks@unimelb.edu.au.

[8] The abbreviations used are: NK, natural killer; TCR, T cell receptor; P, position; CDR, complementarity-determining region; SPR, surface plasmon resonance; BSA, buried surface area; FW, framework; Bistris propane, 1,3-bis[tris(hydroxymethyl)methylamino]propane; LIL, VMAPRTLIL; LVL, VMAPRTLVL; pHLA-E, peptide–HLA-E; V, variable; TRAV, T cell receptor α variable segment; TRBV, T cell receptor β variable segment; TRAJ, T cell receptor α joining region segment; TRBJ, T cell receptor β joining region segment.

T cell recognition of MHC-I proteins and any associated peptide is mediated by the αβ T cell receptor (TCR) via three loops on the α- and β-chains termed complementarity-determining regions (CDRs). However, the majority of the current knowledge of peptide recognition by the TCR is focused on MHC-Ia molecules (3). Nevertheless, there is evidence for distinct roles for T cells restricted by MHC-Ib. For example, in mice, there are numerous MHC-Ib loci, and the MHC-Ib molecules Qa-1^b, Q9, and H2-M3 have been implicated in responses against *Salmonella enterica* serovar Typhimurium (5–7), polyoma virus (8) ,and *Listeria monocytogenes* (9), respectively. Similarly, populations of regulatory cells have been shown to recognize Qa-1^b (10). However, it is unclear whether these T cells recognize their MHC-Ib ligands in an analogous manner to MHC-Ia and whether they elicit qualitatively distinct responses to pathogens. There is evidence that H2-M3–restricted T cells are functionally distinct from those restricted by MHC-Ia both in terms of thymic phenotype and their requirements for activation. For example, H2-M3–restricted T cells appear to be important in the primary immune response following *Listeria* infection but are not expanded upon rechallenge. Furthermore, unlike MHC-Ia–restricted T cells, H2-M3–restricted T cells can be selected on cells of hematopoietic origin (11).

There are far fewer MHC-Ib molecules in humans compared with mice (HLA-E, -F, and -G). Of these, the function of HLA-E is perhaps best understood. It is the least polymorphic of all HLA genes with 17 alleles described to date but with only two alleles dominating, each being present at frequencies of nearly 0.5 (4). Crystal structures of HLA-E have revealed a highly restrictive peptide-binding grove, ideal for accommodating nonamer peptides derived from the leader sequence of other HLA-I proteins (12–14). Indeed, the primary function of HLA-E is to present these peptides to CD94-NKG2 receptors, thus regulating the activity of NK cells. However, HLA-E can also present pathogen-derived peptides from *S. enterica* Typhimurium (6), *Mycobacterium tuberculosis* (15), and human CMV (16, 17) to $CD8^+$ T cells. Moreover, infection of macaques with engineered CMV vectors that expressed HIV type 1 proteins results in HIV-specific, Mamu-E–restricted $CD8^+$ T cell responses (18).

Interestingly, a CMV epitope from the protein UL40 shares an identical amino acid sequence with that found in many but not all HLA-C– derived leader peptides (VMAPRTLIL, or "LIL") and consequently when bound to HLA-E can also promote interactions with CD94-NKG2 receptors (19). In most individuals, the complete sequence identity between these HLA-C– and UL40-encoded peptides likely results in deletional tolerance (20). However, in individuals who lack HLA-C alleles that encode the LIL determinant, robust UL40-specific, $CD8^+$ T cell responses have been observed (17, 21). This UL40-specific T cell response to the LIL epitope appears restricted with the TRBV14 gene segment utilized in a number of T cell clones isolated from several unrelated donors (17, 22).

The structure of a $TRBV14^+$ TCR, called KK50.4, was solved in complex with HLA-E–LIL and showed that the interaction was broadly similar to TCR recognition of MHC-Ia (22). There were, however, a number of distinct features of the TCR/HLA-E interaction. In particular, the CDR2β loop dominated the contacts made with HLA-E. Furthermore, each of the CDR loops of TCRβ made direct contacts with the Ile at position 8 of the peptide (the only peptide residue that differed from self-encoded peptides). To date, the investigation of T cell responses to UL40 have been limited to the prototypical $TRBV14^+$ TCRs that recognize the LIL epitope. However, it remains unclear whether such features are general to TCR recognition of HLA-E–UL40 peptide complexes or to any HLA-E–restricted TCR.

Table 1
Sequences of TCR clones
IMGT nomenclature (40) is used.

	TCR	
	KK50.4	GF4
Donor HLA-Ia	A02, A32, B44, C07	A01, A03, B27, B44, C02
TRAV	26-1*01	35*02
TRAJ	37*02	53*01
Protein sequence CDR1α	TISGNEY	SIFNT
Protein sequence CDR2α	GLKNN	LYKAGEL
Protein sequence CDR3α	CIVVRSSNTGKLIF	CAGQPLGGSNYKLTF
TRBV	14*01	9*01
TRBJ	2-3*01	1-4*01
Protein sequence CDR1β	SGHDN	SGDLS
Protein sequence CDR2β	FVKESK	YYNGEE
Protein sequence CDR3β	CASSQDRDTQYF	CASSANPGDSSNEKLFF

Previous data suggested that the fine specificity of the UL40 T cell response was modified by the presence or absence of HLA-A alleles in the donor that encoded the sequence VMAPRTLVL ("LVL") (17). Notably, in individuals lacking LVL as a self-peptide (*e.g.* donors lacking HLA-A2–type leader peptides), the UL40 T cell response cross-reacted with the LVL peptide. Furthermore, T cells expressing TRBV2 (Vβ22) or TRBV9 (Vβ1), rather than the typical TRBV14, characterized this response. Here, we cloned and expressed a $TRBV9^+$ TCR isolated from such a donor and report two structures of this TCR bound to HLA-E (presenting the LIL and LVL peptides). Using mutagenesis, we determined the energetic contribution of individual HLA-E residues interacting with both the $TRBV9^+$ and $TRBV14^+$ TCRs. Our data suggest that although different TCRs adopt distinct docking modes on HLA-E the energetic basis of the TCR interaction is defined by a set of conserved HLA-E residues.

Results

The GF4 TCR, a non-canonical, $TRBV9^+$, HLA-E–restricted TCR

Previous studies of a canonical $TRVB14^+$ TCR, KK50.4, typical of several HLA-E–restricted UL40-specific T cell clones expanded *in vitro* from unrelated donors (17, 22) demonstrated it to be highly specific for the peptide LIL (17). In contrast, UL40-specific cells isolated from donor GF did not utilize TRBV14 and recognized target cells pulsed with both LIL and LVL peptides with high avidity (17). To assess whether the molecular recognition of HLA-E was conserved between $TRBV14^+$- and non-TRBV14–expressing T cells, we sequenced and cloned the TCR from a T cell clone, GF4, obtained from this donor. The GF4 TCR utilized the TRAV35 and TRBV9 gene segments, and sequence analysis showed the GF4 and KK50.4 TCR CDR3 regions have few elements in common (Table 1). Moreover, the GF4 TCR possessed a longer CDR3β loop than the KK50.4 TCR (15 *versus* 12 amino acids) and

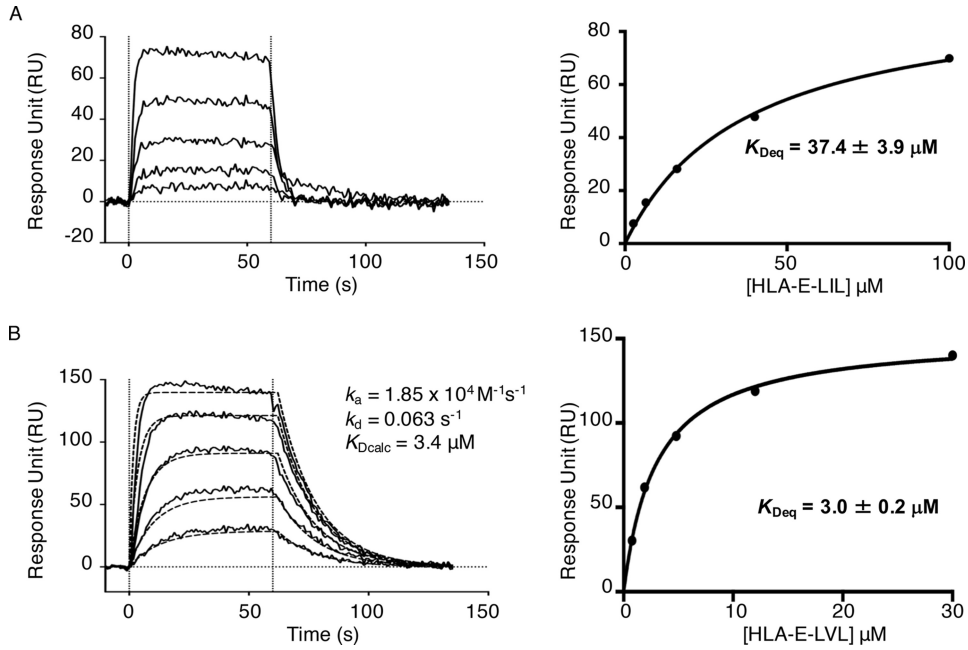

Figure 1. Representative sensorgrams showing the binding of GF4 TCR to peptides presented by HLA-E by surface plasmon resonance. GF4 was captured on the surface of a Bio-Rad ProteOn GLC chip by anti-TCR mAb 12H8 (25) and assessed for its ability to interact with HLA-E presenting LIL or LVL (*A* and *B*, respectively). Increasing concentrations of HLA-E (*A*, 100, 40, 16, 6.4, and 2.6 μM; *B*, 30, 12, 4.8, 1.9, and 0.8 μM) were passed over captured GF4 TCR. K_D was determined by equilibrium analysis (*right panels*) and by kinetic analysis for VMAPRTLVL (*dashed lines* indicate data fit). Data show representative sensorgrams of at least three experiments with independent preparations of refolded proteins.

lacked the conserved $Arg^{110\beta}$ characteristic of $TRBV14^+$ UL40–specific T cell clones (22).

We then determined the affinity of the GF4 TCR for the HLA-E bound to the LIL and LVL peptides by surface plasmon resonance (SPR). GF4 TCR bound to HLA-E–LIL with an affinity of ≈37 μM (Fig. 1*A*) and surprisingly exhibited a 10-fold higher affinity for HLA-E–LVL with a K_D of ≈3 μM (Fig. 1*B*). The higher affinity of the GF4 TCR for the LVL peptide compared with LIL correlated with a slower dissociation rate (Fig. 1). As we had previously determined that the KK50.4 TCR was highly specific for the presence of Ile at P8 (22), the sequence differences between the GF4 and KK50.4 TCRs impacted their peptide specificity.

GF4 TCR binds to HLA-E molecule with an orthogonal docking angle

To define the molecular basis of the interaction between HLA-E and the GF4 TCR, we determined the structures of the GF4 TCR in complex with HLA-E presenting both LIL and LVL peptides (Table 2). The structures of the two GF4 TCR–HLA-E-peptide complexes were similar and aligned with an overall root mean square deviation of 0.49 Å (Fig. 2, *A* and *B*). Here, the GF4 TCR docked centrally on top of the HLA-E cleft with a docking angle of 88° whereupon the TCR β-chain and TCR α-chain were positioned above the α1 and α2 helices, respectively (Fig. 2, *C* and *D*). The buried surface area (BSA) upon complexation was ~2,100 $Å^2$, which falls within the range of previously observed TCR–peptide–MHC-I structures (3).

The BSA was equally distributed between the GF4 TCR α- and β-chains (Fig. 2). All the GF4 TCR CDR loops were involved in the interaction with the HLA-E–peptide complexes (Table 3). The CDR1α, CDR1β loops, and α-chain framework (FWα) had small contributions with BSAs of ~6, ~3, and 4%, respectively, followed by the CDR2α and the FWβ region both contributing to 10% of the BSA. Instead, the interaction was driven by the GF4 TCR CDR3α (~30%), CDR3β (~19%), and CDR2β (~19%) loops (Fig. 2, *C* and *D*).

As the GF4 complexes with both peptides were very similar, we analyze below the GF4 TCR–HLA-E–LVL complex determined at higher resolution (Table 2). The GF4 TCR contacted two large stretches of the α1 and α2 helices from residues 65–80 and 145–158 (Table 3 and Fig. 2*C*). The interaction with the HLA-E α1 helix was largely mediated by the GF4 TCR β-chain (Table 3). Here, all three CDR loops along with $Arg^{66\beta}$, a framework residue, made direct contacts. The CDR1β and

Table 2
Data collection and refinement statistics
Values in parentheses are for the highest-resolution shell. r.m.s.d., root mean square deviation.

	GF4 TCR–HLA-E–LIL	GF4 TCR–HLA-E–LVL
Data collection statistics		
Resolution range (Å)	54.93–3.31 (3.43–3.31)	50.29–3.10 (3.21–3.10)
Space group	$P2_12_12_1$	$P2_12_12_1$
Unit cell (*a*, *b*, *c*) (Å)	71.64, 228.24, 276.87	73.37, 225.92, 276.26
Multiplicity	2.0 (2.0)	2.0 (2.0)
Completeness (%)	99.3 (93.5)	99.8 (100.0)
$I/\sigma(I)$	13.35 (2.75)	10.74 (2.06)
R_{merge} [a] (%)	5.6 (27.8)	6.1 (33.7)
Refinement statistics		
R_{factor} [b] (%)	22.54	21.49
R_{free} [b] (%)	26.81	26.33
r.s.m.d. from ideality		
Bond lengths (Å)	0.015	0.017
Bond angles (°)	1.44	1.76
Ramachandran plot (%)		
Favored	90	93
Outliers	0.85	0.62

[a] $R_{merge} = \Sigma|I_{hkl} - \langle I_{hkl}\rangle|/\Sigma I_{hkl}$.
[b] $R_{factor} = \Sigma_{hkl}||F_o| - |F_c||/\Sigma_{hkl}|F_o|$ for all data except ≈5%, which were used for R_{free} calculation.

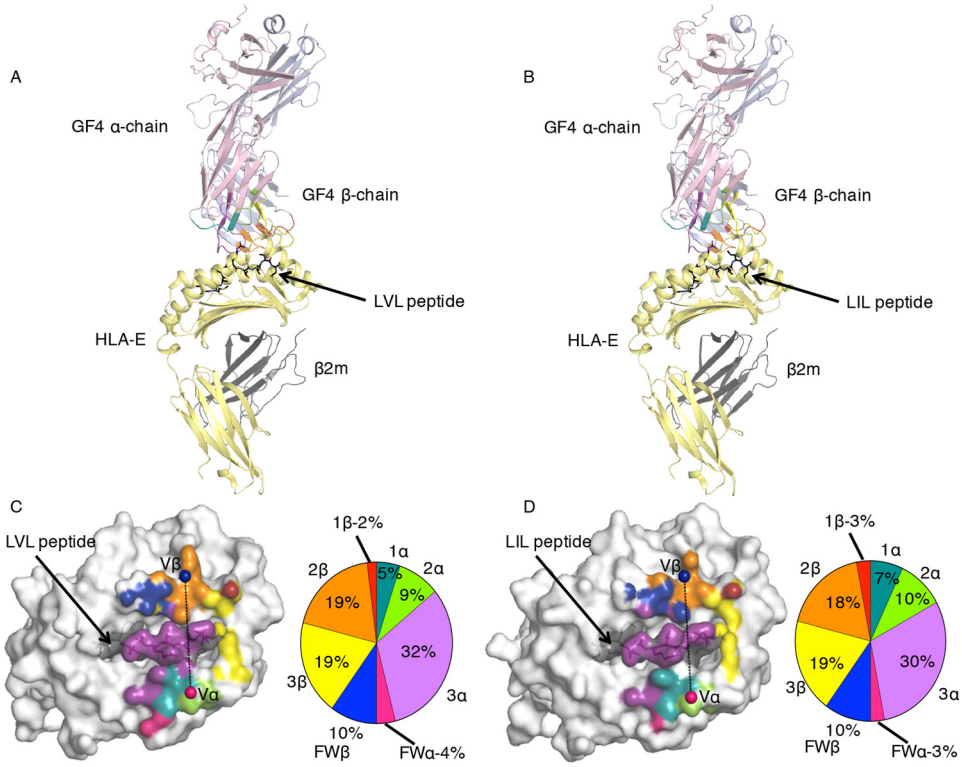

Figure 2. *A* and *B*, the structure of the HLA-E (*yellow* schematic) presenting either LVL (*A*) or LIL (*B*) peptide (*black sticks*) to GF4 TCR (α-chain in *pink* schematic for LIL and β-chain in *blue* schematic); β_2-microglobulin (β_2m) is represented in *gray* schematic. *C* and *D*, structural footprint of the GF4 TCR onto HLA-E–LVL (*C*) or HLA-E–LIL (*D*). The contribution of the CDR loops to the BSA of pHLA-E is represented for GF4 HLA-E–LVL (*C*) and HLA-E–LIL (*D*) complexes. The HLA-E atoms making contacts with CDR1α (*teal*), CDR2α (*green*), CDR3α (*purple*), framework α (*pink*), CDR1β (*red*), CDR2β (*orange*), CDR3β (*yellow*), or framework β (*blue*) are colored accordingly to the TCR segment contacted, whereas the *magenta* and *blue spheres* represent the center of mass for the Vα and Vβ, respectively. The percent contribution of the CDR loops and framework regions of the GF4 TCR–HLA-E–LVL (*C*) and GF4 TCR–HLA-E–LIL (*D*) complexes in binding to the pHLA-E complex is also shown in the *pie charts*.

CDR3β loops formed hydrophobic interactions with the HLA-E heavy chain (Fig. 3*A*) with $Leu^{37\beta}$ interacting with Val^{76} of HLA-E and $Pro^{110\beta}$ binding Arg^{79} and Thr^{80} of the HLA-E heavy chain. The GF4 TCR also made extensive use of CDR2β loop with four of the six residues (^{56}Y**YNGEE**^{65}) alongside $Arg^{66\beta}$, an adjacent FW residue, all being involved in contacting HLA-E. This CDR2-FWβ segment abuts an 11-residue-long stretch of HLA-E (residues 65–76), engaging directly with seven of these residues (Table 3). This region of the HLA-E α1 helix is highly charged with four Arg and one Asp residue interacting with the two Glu residues and one Arg of the CDR2-FWβ segment, thereby forming an extensive salt-bridging network (Table 3 and Fig. 3*B*). A large network of hydrogen bonds and hydrophobic contacts further strengthened the GF4/HLA-E interaction (Table 3). Here, the side chain of $Tyr^{57\beta}$ of the CDR2β loop was lodged between the Val^{76} and Ile^{73} of HLA-E, forming a peg/notch interaction (Fig. 3*C*). Similarly, the side chain of the FW residue $Arg^{66\beta}$ inserted its guanidinium group between the side chains of Asp^{69}/Gln^{72} and the CDR3α loop (Fig. 3*D*). Altogether, this highlights the important contribution of the GF4 TCR β-chain in interacting with the HLA-E molecule (Fig. 2*C*).

TCR recognition of the HLA-E α2 helix was mainly mediated by the TCR α-chain (Table 3). All three CDRα loops along with a framework residue, $Arg^{84\alpha}$, contacted the α2 helix (Table 3). The GF4 TCR α-chain contacted the center of the α2 helix either side of the hinge region spanning residues 150–155, highlighting the central docking mode of the TCR onto the HLA-E molecule (Fig. 2*C*). The CDR1α formed hydrophobic interactions with Ala^{150}, Glu^{154}, and His^{155} as well as being within hydrogen-bonding distance to the main chain of Ser^{150} (Fig. 3*E*). Most of the CDR2α contacts were mediated via the $Tyr^{57\alpha}$ whose aromatic side chain lay flat on the hinge of the α2 helix, whereas the FWα residue $Arg^{84\alpha}$ formed a salt bridge with Glu^{154} (Fig. 3*E*). The interactions between the CDR3α loop and HLA-E were focused around the His^{155} residue. The ^{107}QPLGG^{111} residues of the CDR3α loop surrounded the His^{155} side chain, which was further caged by the $Asn^{37\alpha}$ and the P5 Arg from the peptide. The "cage" surrounding His^{155} is closed by interaction between $Gln^{107\alpha}$ and Glu^{152} of HLA-E, which fully buried the α2 helix residue upon binding of the GF4 TCR (Fig. 3*F*). Hence, our structural analysis showed that the GF4 TCR used all six CDR loops as well as FW residues from both chains to engage the two helices of the HLA-E in an orthogonal docking mode.

The GF4 TCR interaction with the LVL and LIL peptides is driven by the CDR3α loop

The GF4 TCR bound to a large stretch of the peptide, ranging from P4 Pro to P9 Leu (Table 3). The majority of the contacts were made by the CDR3α loop (87% BSA), whereas the CDR3β loop made a smaller contribution (13% BSA) (Table 3). The CDR3β formed a salt bridge with the P5 Arg via $Glu^{116\beta}$, whereas $Pro^{110\beta}$ and $Asn^{115\beta}$ both contacted the P8 Val residue

Table 3

Contacts of GF4 TCR–HLA-E–LIL, GF4 TCR–HLA-E–LVL, and KK50.4 TCR–HLA-E–LIL (22) complex interactions

HB, hydrogen bonds (cutoff at 3.5 Å); SB, salt bridge (cutoff at 5 Å); VDW, van der Waals (cutoff at 4.5 Å).

	GF4–HLA-E–LIL	GF4–HLA-E–LVL	KK50.4–HLA-E–LIL	Type of bond
HLA-E				
Arg^{62}			$Arg^{108\alpha}$	VDW
Arg^{65}	$Arg^{66\beta}$, $Ala^{67\beta}$	$Arg^{66\beta}$	$Asp^{67\beta}$	HB, SB, VDW
Arg^{68}		$Glu^{65\beta}$, $Arg^{66\beta}$		HB, SB, VDW
Asp^{69}	$Ser^{112\alpha}$	$Ser^{112\alpha}$	$Asn^{112\alpha}$, $Thr^{113\alpha}$	HB, VDW
	$Arg^{66\beta}$	$Arg^{66\beta}$	$Gln^{66\beta}$	HB, VDW
Thr^{70}			$Asn^{112\alpha}$	VDW
Gln^{72}	$Tyr^{57\beta}$, $Glu^{64\beta}$, $Glu^{65\beta}$, $Arg^{66\beta}$	$Tyr^{57\beta}$, $Glu^{64\beta}$, $Glu^{65\beta}$, $Arg^{66\beta}$	$Gln^{66\beta}$	HB, VDW
Ile^{73}	$Asn^{113\alpha}$, $Tyr^{114\alpha}$	$Asn^{113\alpha}$, $Tyr^{114\alpha}$		VDW
	$Tyr^{57\beta}$, $Arg^{66\beta}$	$Tyr^{57\beta}$, $Arg^{66\beta}$	$Val^{57\beta}$, $Gln^{66\beta}$	VDW
Arg^{75}	$Asn^{58\beta}$, $Glu^{64\beta}$	$Asn^{58\beta}$, $Glu^{64\beta}$	$Ser^{64\beta}$	SB, HB, VDW
Val^{76}	$Leu^{37\beta}$, $Tyr^{57\beta}$, $Asn^{58\beta}$, $Pro^{110\beta}$	$Leu^{37\beta}$, $Tyr^{57\beta}$, $Asn^{58\beta}$, $Pro^{110\beta}$	$Val^{57\beta}$, $Ser^{64\beta}$	VDW
Arg^{79}	$Leu^{37\beta}$, $Pro^{110\beta}$	$Leu^{37\beta}$, $Pro^{110\beta}$	$Glu^{63\beta}$	SB, VDW
Thr^{80}	$Pro^{110\beta}$	$Pro^{110\beta}$	$Lys^{58\beta}$	VDW
Gln^{145}		$Ser^{113\beta}$		HB, VDW
Lys^{146}	$Pro^{110\beta}$, $Asp^{112\beta}$, $Ser^{113\beta}$, $Asn^{115\beta}$	$Pro^{110\beta}$, $Asp^{112\beta}$, $Ser^{113\beta}$, $Asn^{115\beta}$	$Asp^{37\beta}$	HB, SB, VDW
Asn^{148}	$Lys^{58\alpha}$	$Lys^{58\alpha}$		HB, VDW
Asp^{149}	$Tyr^{57\alpha}$	$Tyr^{57\alpha}$		VDW
Ala^{150}	$Asn^{37\alpha}$, $Thr^{38\alpha}$, $Tyr^{57\alpha}$	$Asn^{37\alpha}$, $Thr^{38\alpha}$, $Tyr^{57\alpha}$	$Asp^{109\beta}$	VDW
Ser^{151}	$Asn^{37\alpha}$, $Tyr^{57\alpha}$, $Lys^{58\alpha}$	$Asn^{37\alpha}$, $Tyr^{57\alpha}$, $Lys^{58\alpha}$		HB, VDW
Glu^{152}		$Gln^{107\alpha}$, $Asn^{113\alpha}$	$Asp^{109\beta}$, $Arg^{110\beta}$	SB, VDW
Glu^{154}	$Asn^{37\alpha}$, $Arg^{84\alpha}$, $Leu^{109\alpha}$	$Asn^{37\alpha}$, $Arg^{84\alpha}$, $Leu^{109\alpha}$	$Tyr^{38\alpha}$, $Leu^{57\alpha}$	SB, HB, VDW
His^{155}	$Asn^{37\alpha}$, $Gln^{107\alpha}$, $Pro^{108\alpha}$, $Leu^{109\alpha}$, $Gly^{110\alpha}$	$Asn^{37\alpha}$, $Gln^{107\alpha}$, $Pro^{108\alpha}$, $Leu^{109\alpha}$, $Gly^{110\alpha}$, $Gly^{111\alpha}$	$Tyr^{38\alpha}$, $Tyr^{40\alpha}$, $Ser^{109\alpha}$, $Asp^{111\beta}$	HB, VDW
Arg^{157}		$Arg^{84\alpha}$	$Leu^{57\alpha}$	VDW
Ala^{158}	$Leu^{109\alpha}$	$Leu^{109\alpha}$	$Tyr^{38\alpha}$	VDW
Asp^{162}			$Gly^{30\alpha}$	VDW
Peptide				
P4 Pro	$Gly^{110\alpha}$, $Ser^{112\alpha}$	$Gly^{110\alpha}$, $Ser^{112\alpha}$	$Ser^{109\alpha}$, $Ser^{110\alpha}$	VDW
P5 Arg	$Gln^{107\alpha}$, $Pro^{108\alpha}$, $Gly^{110\alpha}$, $Gly^{111\alpha}$, $Ser^{112\alpha}$, $Asn^{113\alpha}$, $Tyr^{114\alpha}$	$Gln^{107\alpha}$, $Pro^{108\alpha}$, $Gly^{110\alpha}$, $Gly^{111\alpha}$, $Ser^{112\alpha}$, $Asn^{113\alpha}$, $Tyr^{114\alpha}$	$Ser^{110\alpha}$, $Asn^{111\alpha}$	HB, VDW
	$Glu^{116\beta}$	$Glu^{116\beta}$	$Asn^{109\beta}$, $Arg^{110\beta}$, $Asn^{112\beta}$	HB, SB, VDW
Thr^{6}	$Asn^{113\alpha}$	$Asn^{113\alpha}$	$Asn^{112\alpha}$	HB, VDW
			$Arg^{110\beta}$	HB, VDW
Leu^{7}		$Asn^{113\alpha}$		VDW
Ile/Val^{8}	$Asn^{113\alpha}$, $Tyr^{114\alpha}$	$Asn^{113\alpha}$, $Tyr^{114\alpha}$		VDW
	$Glu^{116\beta}$	$Pro^{110\beta}$, $Asn^{115\beta}$	$Asp^{37\beta}$, $Asn^{38\beta}$, $Val^{57\beta}$, $Arg^{110\beta}$	VDW
Leu^{9}	$Pro^{110\alpha}$	$Pro^{110\alpha}$		VDW

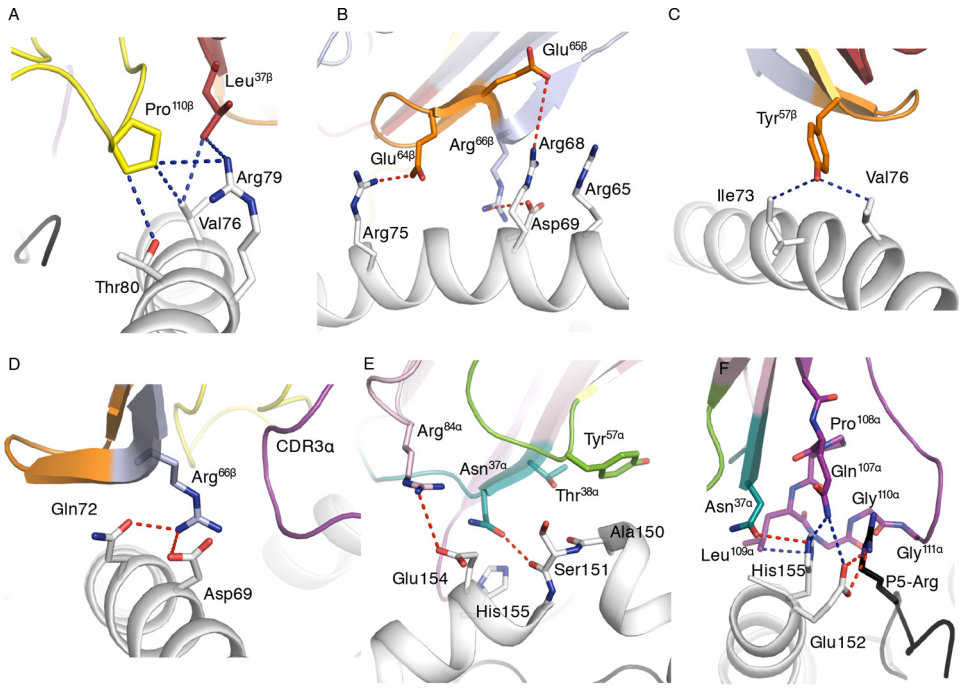

Figure 3. *A–D*, GF4 TCR β-chain interactions with HLA-E (*white*) via the CDR1β (*red*) and CDR3β residues (*yellow*) (*A*) via the CDR2β (*orange*) framework β (*pale blue*) (*B*, *C*, and *D*). *E* and *F*, GF4 TCR α-chain interactions with HLA-E α2 helix via the CDR1α (*teal*), CDR2α (*green*), and framework α (*pale pink*) (*E*) as well as via the CDR3α (*purple*) (*F*). Residues interacting are depicted as *sticks*, hydrophobic bonds are shown as *blue dashed lines*, and salt bridges or hydrogen bonds are shown as *red dashed lines*.

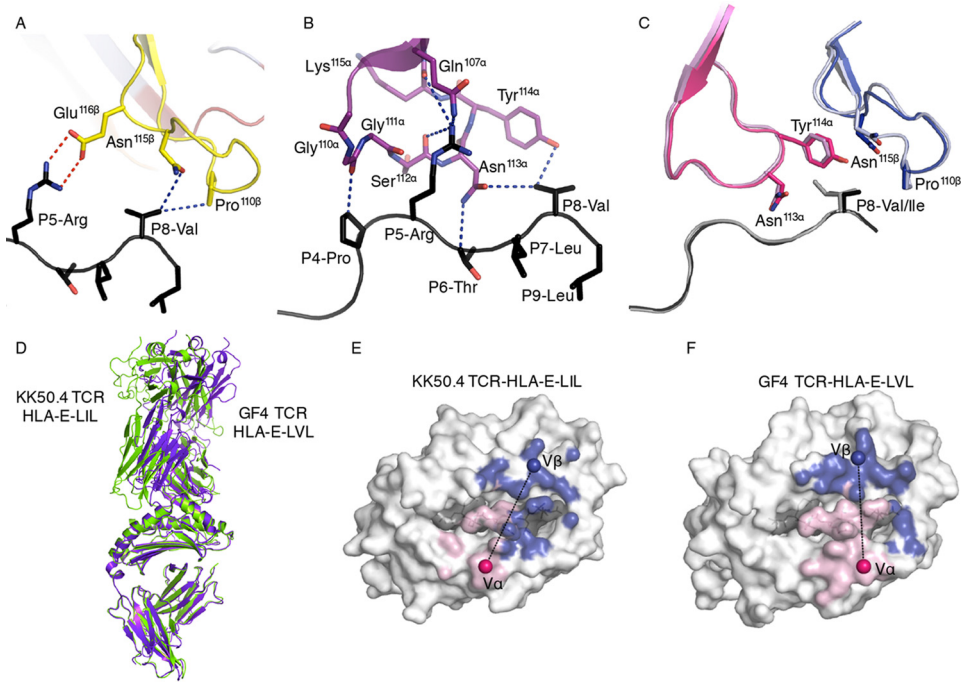

Figure 4. *A–C*, GF4 TCR interactions with the peptides: LVL peptide (*black stick*) interactions with CDR3β (*yellow*) (*A*) and CDR3α (*purple*) (*B*). Superimposition of GF4 TCR CDR3 loops in complex with the HLA-E–LIL and HLA-E–LVL is shown in *C* with the CDR3α loops in *pink*, CDR3β loops in *blue* for the GF4 TCR–HLA-E–LVL and *lighter shade* for the GF4 TCR–HLA-E–LIL, and the peptides in *black* (LVL) and *gray* (LIL). Residues interacting are depicted as *sticks*, hydrophobic bonds are shown as *blue dashed lines*, and salt bridges are shown as *red dashed lines*. *D*, superimposition of KK50.4 TCR–HLA-E–LIL (*green* schematic) and GF4 TCR–HLA-E–LVL (*purple* schematic). *E* and *F*, structural footprint of KK50.4 TCR onto HLA-E–LIL (*E*) and GF4 TCR onto HLA-E–LVL (*F*). The pHLA-E atoms making contacts with each TCR are shown in *light pink* (α-chain) and *blue* (β-chain). The *magenta* and *blue spheres* represent the center of mass for the Vα and Vβ, respectively.

in the LVL peptide (Fig. 4*A*) and formed similar contacts with the P8 Ile with the LIL peptide (Table 3). In addition, $Pro^{110\beta}$ made contacts with P9 Leu (Table 3). The CDR3α loop made an extensive series of contacts whereupon P5 Arg of the peptide was encompassed by the ^{110}GGSNYK^{115} region of the CDR3α loop and further encaged at the top by $Gln^{107\alpha}$ that was within hydrogen-bonding distance with P5 Arg. The CDR3α loop was positioned above the P4 Pro and the backbone of the P6 Thr and P7 Leu. Moreover, $Tyr^{114\alpha}$ contacted the side chain of the P8 Val of the LVL peptide, which was also contacted by $Asn^{113\alpha}$ (Fig. 4*B*). As such, the P8 Val was fully buried upon binding of the GF4 TCR. Analysis of GF4 bound to the HLA-E–LIL complex showed a similar set of contacts, although the larger P8 Ile created a ripple of small structural adjustments within the CDR3 loops (Fig. 4*C*) to accommodate the additional methyl group, which might be sufficiently less favorable for binding to the GF4 TCR and account for the affinity differences (Fig. 1). Hence, the GF4 TCR engaged the peptide with a large footprint driven by the CDR3α loop.

Structural comparison of KK50.4 TCR and GF4 TCR in complex with HLA-E

Despite the GF4 and KK50.4 TCRs (22) engaging with the same monomorphic HLA-E molecule, the differing V gene segment usage (Table 1) between the TCRs was associated with differences in the molecular architecture of the TCR/HLA-E interaction (Fig. 4*D*). Notably, the KK50.4 TCR is heavily reliant (60% of contacts) on the TCR β-chain to engage with the HLA-E–LIL (Fig. 4*E*) (22), whereas the GF4 TCR uses both chains to a similar extent (Fig. 4*F*). The BSA is larger in the complex with the GF4 TCR (2,100 Å^2) compared with the KK50.4 TCR (1,800 Å^2). Moreover, the docking angles are markedly different with a diagonal docking for the KK50.4 TCR (56°) (Fig. 4*E*) and an orthogonal docking for the GF4 TCR (88°) (Figs. 2, *C* and *D*, and 4*F*). Although the center of mass of the β-chains from each TCR aligned well (Fig. 4, *E* and *F*), the α-chain of the GF4 TCR made a ~30° shift toward the C-terminal end of the antigen-binding cleft compared with the KK50.4 TCR. In addition, although both the α- and β-chains of KK50.4 TCR contacted the LIL peptide and the α2 helix of the HLA-E (Fig. 4*E*), the GF4 TCR largely used the TCR α-chain to interact with these parts of the HLA-E–peptide complex (Fig. 4*F*).

The GF4 and KK50.4 TCRs contacted 22 and 19 HLA-E residues, respectively, 15 of which were shared, albeit interacting with different TCR residues (Table 3). Here, the CDR2β loops were shifted by ~5 Å between the two TCRs. Despite this docking difference, the side chains of two residues (57 and 66) from the CDR2β-FWβ segment made similar contacts with the HLA-E molecule; $Val^{57\beta}$ and $Tyr^{57\beta}$ of KK50.4 and GF4 TCRs, respectively, lodged their side chains between Ile^{73} and Val^{76} of the HLA-E molecule (Fig. 5*C*), whereas the FWβ residue at position 66 (Arg and Gln from GF4 and KK50.4 TCRs, respectively), pointed its side chain toward Asp^{69}, Gln^{72}, and Ile^{73} (Fig. 5*C*).

Although the CDR3α loops of GF4 and KK50.4 TCRs were located similarly above P4 Pro and surrounded the P5 Arg side chain (Fig. 5*A*), the GF4 TCR CDR3α loop (BSA of ~30%) contributed double the BSA of the KK50.4 TCR CDR3α loop (BSA of 14%) (22). This higher contribution of the GF4 TCR CDR3α

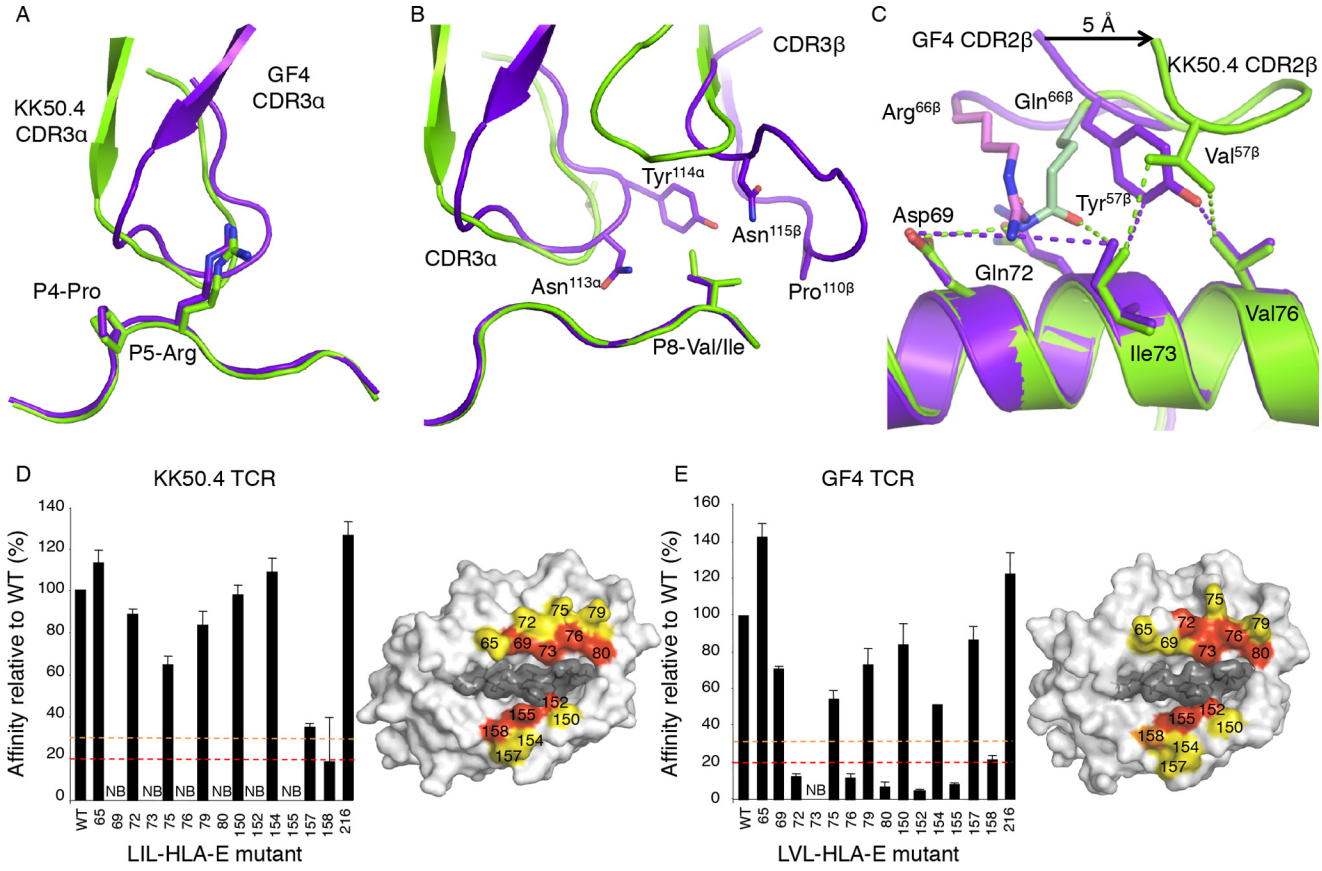

Figure 5. Superimposition of the KK50.4 TCR–HLA-E–LIL (*green*) and GF4 TCR–HLA-E–LVL (*purple*) structures with the CDR3α loops surrounding the P4-P5 peptide residues (*A*) and the CDR3 loops around the P8 position of the peptides (*B*) is shown. *C* shows a superposition of the KK50.4 (*green*) and GF4 (*purple*) TCR CDR2β loops and their interactions with the HLA-E molecule; the *lighter shade*-colored residues are from the framework β segment. The *dashed lines* indicate the interactions between residues in each complex. Affinity of HLA-E mutants to KK50.4 TCR (*D*) or GF4 TCR (*E*) is represented as relative percentage of the wild-type (WT) value determined by surface plasmon resonance as well as the energetic footprints of each TCR on HLA-E. *Dotted lines* represent 30% (or 3 times binding reduction) in *orange* and 20% (or 5 times binding reduction) in *red* of the binding affinity compared with WT HLA-E. The effect of each mutation (*yellow*, no effect; *orange*, 3 times binding reduction; *red*, 5 times binding reduction) is represented on the HLA-E surface. Peptides residues are shown in *gray*. *Error bars* represent S.E.

loop was associated with $Tyr^{114\alpha}$ sitting above the P8 Val residue of the LVL peptide (Fig. 5*B*). However, the area surrounding the P8 residue of the peptide formed by the CDRβ loops of KK50.4 was larger than that in the GF4 TCR and therefore might accommodate a P8 Ile more favorably than a P8 Val (Fig. 5*B*). The comparison of the GF4 and KK50.4 structures in complex with HLA-E–peptide showed that despite disparate TCR gene usage and differing docking strategies a similar set of HLA-E and peptide residues formed the TCR recognition site.

Shared energetic footprint between KK50.4 and GF4 TCRs onto the monomorphic HLA-E molecule

Although both the GF4 and KK50.4 TCRs interacted with a similar set of residues on HLA-E, the relative energetic contributions of these HLA-E residues toward TCR recognition was unclear. Consequently, based on the structures of the TCR–HLA-E–peptide complexes, we mutated the HLA-E residues engaged by both TCRs (Table 3) (with the exception of Lys^{146} that is also critical for peptide binding) (23). Each residue was substituted to an alanine with the exception of Ala^{150} and Ala^{158}, which were mutated to glycine. In addition to the 14 HLA-E residues mutated, we also mutated a residue outside of the binding cleft, Thr^{216}, as a negative control. We tested the affinity, as determined by SPR, of these 15 HLA-E mutants for both the GF4 and KK50.4 TCRs in the presence of their high-affinity peptides LVL and LIL, respectively (Fig. 5, *D* and *E*). The impact of each mutation was classified as follows: no effect if the affinity was decreased less than 3-fold, a moderate effect if the affinity was decreased by 3–5-fold, or a dramatic impact if the affinity was decreased by more than 5-fold compare with the wild-type HLA-E. First, the T216A mutant, used as negative control, did not impact the affinity of either the GF4 or KK50.4 TCRs. The affinity between wild-type HLA-E and KK50.4 was ~25 μM (mean of three independent experiments, 26.7 ± 1.3 μM; data not shown), similar to results reported previously (22).

Of the 15 substitutions tested, seven (R65A, Q72A, R75A, R79A, A150G, E154A, and R157A) had no significant effect on the affinity of interaction with the KK50.4 TCR, whereas mutation of seven residues (D69A, I73A, V76A, T80A, E152A, H155A, and A158G) had a marked effect upon recognition by KK50.4 TCR (Fig. 5*D*). Similarly, seven of these substitutions (R65A, D69A, R75A, R79A, A150G, E154A, and R157A) had little impact on the GF4 TCR binding with one having a moderate impact (A158G) and six (Q72A, I73A, V76A, T80A, E152A, and H155A) dramatically impacting the affinity of GF4 TCR for the HLA-E–LVL complex (Fig. 5*E*). Noticeably, 11 of

the 15 substitutions on the HLA-E molecule impacted the affinity in the same fashion despite the difference in the interactions with the respective TCR–HLA-E interfaces (Fig. 4, *F* and *E*). Of the substitutions that equally impacted TCR affinity, five decreased the affinity by more than 5-fold, two on the α2 helix (E152A and H155A) and three on the α1 helix (I73A, V76A, and T80A) (Fig. 5, *D* and *E*), thereby representing a common "hot spot" for recognition by the two TCRs with divergent gene usage.

Discussion

Of the MHC-Ib molecules found in humans, only HLA-E has been shown to bind to the αβ TCR expressed by CD8 T cells. Indeed there has been significant interest in HLA-E–restricted T cells as a result of CMV vector-based vaccination strategies that elicit protective Mamu-E–restricted T cell responses specific for pathogens such as HIV in macaques (18). However, because there is only one crystal structure of HLA-E in complex with a TCR, our understanding of TCR recognition of HLA-E and MHC-Ib molecules more broadly remains extremely limited. Here, we describe two additional TCR–HLA-E–peptide structures and have assessed the energetic contribution of individual HLA-E residues to TCR binding. Our findings show that different TCR gene usage results in distinct TCR docking mechanisms onto HLA-E.

We had previously observed that the affinity of KK50.4 TCR for HLA-E was relatively low compared with many other MHC-Ia–virus-specific TCRs (22). We proposed that this in part may have been due to the near sequence identity between the cognate CMV-derived peptide-ligand– and self HLA-I–leader sequence– encoded peptides expressed in the donor thymus that differed by only a single methyl group (VMAPRTLIL *versus* VMAPRTLVL). Donor GF was somewhat distinct, lacking HLA-I alleles that encode both VMAPRTLIL and VMAPRTLVL. We hypothesized that in such donors there is greater scope to select TCRs with specificity for CMV-encoded peptides. This would potentially increase the repertoire of TCR and the likelihood of TCR with higher affinity for antigen being selected as a result of more relaxed negative selection. Consistent with this, the GF4 TCR bound the HLA-E–LVL complex with significantly higher affinity than the KK50.4 bound to the HLA-E–LIL complex.

A number of studies have shown polymorphisms in this region of the UL40 gene. We reported that only half of the UL40 sequences isolated from a cohort of hematopoietic stem cell transplant recipients possessed the canonical VMAPRTLIL epitope, and the variants VMAPRTLLL and VMAPRTLVL were found in 16 and 12% of patients, respectively (15). Indeed, although the vast majority of research on UL40-specific T cells has focused on those that recognize the canonical VMAPRTLIL peptide, the polymorphism in this region of UL40 suggests that the capacity to generate HLA-E–restricted UL40-specific T cells may not be strictly limited to individuals with specific HLA-C types. The ability of individuals to produce such cells will depend not only on the HLA-Ia alleles present that likely shape the HLA-E–restricted, UL40-specific repertoire but also on the UL40 sequence present within the CMV strain.

The different TRAV and TRBV usage as well as the altered docking orientations between KK50.4 and GF4 indicates that HLA-E is capable of selecting T cells that express distinctly different TCRs into the immune repertoire. Interestingly, despite the sequence and structural differences, these TCRs utilized a similar energetic hot spot of recognition on HLA-E. This is in contrast to previous finding of TCR recognition of MHC-Ia where different structural footprints can result in altered energetic footprints (23). Significantly, here we have demonstrated that approximately half of the HLA-E contact residues are critical for binding to both the KK50.4 and GF4 TCRs. This, in general, is in contrast with the smaller energetic footprints that can underpin TCR–MHC-I recognition (24, 25). Nevertheless, previous studies have identified position 155 in the MHC-Ia heavy chain as well as the MHC-II– equivalent residue 70β as often (but not always) representing a critical position for TCR recognition of MHC (26–29). The loss of KK50.4 and GF4 recognition of HLA-E caused by the H155A mutation is consistent with the importance of this position.

HLA-E is more conserved in evolution than classical HLA-I with the gene arising prior to primate evolution, presumably becoming fixed as a consequence of acting as a ligand for CD94-NKG2 receptors (30, 31). We have previously assessed the ability of mutant HLA-E molecules to interact with the inhibitory NK cell receptor CD94-NKG2A and shown that this innate recognition of HLA-E was also characterized by a broad energetic footprint with seven of 11 of the contact residues contributing to the binding energy (32, 33). Given that a large number of HLA-E residues are critical to the interaction with both NK cell receptors and TCRs, it is possible that the energetic principles governing immune recognition of MHC-Ib may be more stringent. In any case, our data indicate that the rules governing TCR recognition of MHC-Ia molecules may not always be applicable to the less polymorphic MHC-Ib molecules.

Experimental procedures

Generation of recombinant HLA-E

cDNA encoding the extracellular domain of wild-type HLA-E*0103 and human β_2-microglobulin were cloned into the pET-30 expression vector. The proteins were refolded with the synthetic peptide VMAPRTLIL (LIL) or VMAPRTLVL (LVL) (GenScript) as described (22). The resulting complexes were purified by anion-exchange and gel-filtration chromatography. Mutations were introduced into the HLA-E heavy chain by the QuikChange® site-directed mutagenesis kit (Stratagene La, Jolla, CA), and the sequence of the mutated HLA-E cDNA was verified by DNA sequencing. HLA-E mutants were expressed in *Escherichia coli* with yields similar to the wild-type HLA-E and an appearance identical to the wild-type HLA-E heavy chain when inclusion bodies were separated by SDS-PAGE (data not shown). Moreover, mutants eluted from size-exclusion columns at the same volume as wild-type HLA-E and were each recognized by the pan-HLA class I mAb w6/32 and an anti-human β_2-microglobulin antibody in a capture ELISA (data not shown) (34).

Generation of recombinant TCR

Soluble, recombinant forms of the UL40-specific TCRs KK50.4 and GF4 were generated essentially as described previously (22). Briefly, the α- and β-chains of the TCRs were cloned separately into the pET-30 expression vector, expressed and purified from inclusion bodies, and then refolded by dilution in a buffer containing 5 M urea. The resulting αβ TCR complex was purified by anion-exchange, gel-filtration, and Mono Q chromatography.

Surface plasmon resonance

SPR experiments were performed as described previously (22). Experiments were conducted at 25 °C either on a BIAcore 3000 or Bio-Rad ProteOn instrument at a flow rate of 20 (BIAcore) or 30 μl/min (ProteOn). Both the running and sample buffers were 10 mM HEPES (pH 7.4), 150 mM NaCl, and 0.05% Tween 20 plus 1% bovine serum albumin to inhibit nonspecific binding. The machines yielded consistent binding affinities across the different platforms. The antibody 12H8 that is specific for the constant region of TCR αβ (25) was coupled to all flow cells of a CM5 (BIAcore) or GLC (ProteOn) chip. For each experiment, two different preparations of either KK50.4 or GF4 TCR were passed over two different flow cells, and ~300–500 response units of the TCR was captured by the antibody. The other flow cells served as control cells for the experiments. Wild-type HLA-E or HLA-E mutants were injected over all flow cells at a concentration range of 1.8–100 μM. The antibody surface was regenerated between each analyte injection with ActiSep (Sterogene) or glycine HCl (pH 3) (Bio-Rad). All measurements were minimally done in duplicate. BIAevaluation version 3.1 or ProteOn Manger version 2.1 was used for data analysis, and data were fitted using the 1:1 Langmuir binding model.

Crystallization, data collection, and structure determination

Crystals of the GF4 TCR in complex with HLA-E–LVL (10 mg/ml) or with HLA-E–LIL (10 mg/ml) in 10 mM Tris-HCl (pH 8) and 150 mM NaCl buffer were grown at 20 °C by the hanging-drop, vapor-diffusion method with a protein/reservoir drop ratio of 1:1. Crystals of GF4 TCR–HLA-E–VMAPRTLVL and GF4 TCR–HLA-E–VMAPRTLIL were obtained in 0.2 M potassium sodium tartrate, 0.1 M Bistris propane (pH 8.0), and 20% PEG3350 (w/v). Crystals were soaked in a cryoprotectant solution containing mother liquor solution supplemented with 20% PEG3350 (w/v) and flash frozen in liquid nitrogen. All data sets were collected on the MX2 beamlines at the Australian Synchrotron, Clayton, Australia using the Area Detector Systems Corp. Quantum 315r charge-couple device detectors (at 100 K). Data sets were processed with MOSFLM software (35) and scaled using SCALA software (International Standard Serial Number 0907-4449) from the CCP4 suite (36). Both GF4 TCR–HLA-E–LVL and GF4 TCR–HLA-E–LIL structures were determined by molecular replacement using the PHASER program with the LC13 TCR (Protein Data Bank code 1KGC (37)) and unliganded HLA-E–VMAPRTLIL (Protein Data Bank code 2ESV (22)) as search models.

Manual model building was conducted using Coot software (38) followed by maximum-likelihood refinement with BUSTER (39). The GF4 TCR was numbered according to the IMGT unique numbering system (40). The final models were validated using the Protein Data Base validation web site, and the final refinement statistics are presented in Table 1. Coordinates for GF4 TCR–HLA-E–LVL (code 5W1W) and GF4 TCR–HLA-E–LIL (code 5W1V) were submitted to the Protein Data Bank. All molecular graphics representations were created using PyMOL (41).

Author contributions—L. C. S. cloned TCRs and mutant HLA-E, made recombinant proteins, conducted the SPR and mutagenesis experiments, analyzed the results, and wrote the manuscript. N. G. W. made recombinant proteins and conducted data collection, structural refinement, and analysis. C. F. and S. G. conducted structural refinement and structural analysis and drafted the paper. G. P. isolated and expanded T cells clones. C. S. C. assisted in structural refinement. M. J. W. S. and E. J. L. produced recombinant proteins and assisted in SPR experiments. T. B. assisted in SPR experiments. M. F. sequenced DNA from T cell clones. M. C. M. and L. M. provided intellectual input. J. R. and A. G. B. assisted in drafting the manuscript and provided important intellectual input. All authors analyzed the results and approved the final version of the manuscript.

Acknowledgments—We thank the staff at the Monash Macromolecular Crystallisation Facility and the Australian Synchrotron MX1 and MX2 beamlines for expert assistance.

References

1. Davis, M. M., and Bjorkman, P. J. (1988) T-cell antigen receptor genes and T-cell recognition. *Nature* **334,** 395–402
2. Sullivan, L. C., Hoare, H. L., McCluskey, J., Rossjohn, J., and Brooks, A. G. (2006) A structural perspective on MHC class Ib molecules in adaptive immunity. *Trends Immunol.* **27,** 413–420
3. Rossjohn, J., Gras, S., Miles, J. J., Turner, S. J., Godfrey, D. I., and McCluskey, J. (2015) T cell antigen receptor recognition of antigen-presenting molecules. *Annu. Rev. Immunol.* **33,** 169–200
4. Grimsley, C., Kawasaki, A., Gassner, C., Sageshima, N., Nose, Y., Hatake, K., Geraghty, D. E., and Ishitani, A. (2002) Definitive high resolution typing of HLA-E allelic polymorphisms: identifying potential errors in existing allele data. *Tissue Antigens* **60,** 206–212
5. Lo, W. F., Ong, H., Metcalf, E. S., and Soloski, M. J. (1999) T cell responses to Gram-negative intracellular bacterial pathogens: a role for CD8+ T cells in immunity to *Salmonella* infection and the involvement of MHC class Ib molecules. *J. Immunol.* **162,** 5398–5406
6. Salerno-Gonçalves, R., Fernandez-Viña, M., Lewinsohn, D. M., and Sztein, M. B. (2004) Identification of a human HLA-E-restricted CD8+ T cell subset in volunteers immunized with *Salmonella enterica* serovar Typhi strain Ty21a typhoid vaccine. *J. Immunol.* **173,** 5852–5862
7. Soloski, M. J., and Metcalf, E. S. (2001) The involvement of class Ib molecules in the host response to infection with *Salmonella* and its relevance to autoimmunity. *Microbes Infect.* **3,** 1249–1259
8. Swanson, P. A., 2nd, Pack, C. D., Hadley, A., Wang, C. R., Stroynowski, I., Jensen, P. E., and Lukacher, A. E. (2008) An MHC class Ib-restricted CD8 T cell response confers antiviral immunity. *J. Exp. Med.* **205,** 1647–1657
9. Lenz, L. L., Dere, B., and Bevan, M. J. (1996) Identification of an H2-M3-restricted *Listeria* epitope: implications for antigen presentation by M3. *Immunity* **5,** 63–72
10. Sarantopoulos, S., Lu, L., and Cantor, H. (2004) Qa-1 restriction of CD8+ suppressor T cells. *J. Clin. Investig.* **114,** 1218–1221
11. Urdahl, K. B., Sun, J. C., and Bevan, M. J. (2002) Positive selection of MHC class Ib-restricted $CD8^+$ T cells on hematopoietic cells. *Nat. Immunol.* **3,** 772–779

12. Hoare, H. L., Sullivan, L. C., Clements, C. S., Ely, L. K., Beddoe, T., Henderson, K. N., Lin, J., Reid, H. H., Brooks, A. G., and Rossjohn, J. (2008) Subtle changes in peptide conformation profoundly affect recognition of the non-classical MHC class I molecule HLA-E by the CD94-NKG2 natural killer cell receptors. *J. Mol. Biol.* **377,** 1297–1303
13. O'Callaghan, C. A., Tormo, J., Willcox, B. E., Braud, V. M., Jakobsen, B. K., Stuart, D. I., McMichael, A. J., Bell, J. I., and Jones, E. Y. (1998) Structural features impose tight peptide binding specificity in the nonclassical MHC molecule HLA-E. *Mol. Cell* **1,** 531–541
14. Strong, R. K., Holmes, M. A., Li, P., Braun, L., Lee, N., and Geraghty, D. E. (2003) HLA-E allelic variants. Correlating differential expression, peptide affinities, crystal structures, and thermal stabilities. *J. Biol. Chem.* **278,** 5082–5090
15. Joosten, S. A., van Meijgaarden, K. E., van Weeren, P. C., Kazi, F., Geluk, A., Savage, N. D., Drijfhout, J. W., Flower, D. R., Hanekom, W. A., Klein, M. R., and Ottenhoff, T. H. (2010) *Mycobacterium tuberculosis* peptides presented by HLA-E molecules are targets for human CD8 T-cells with cytotoxic as well as regulatory activity. *PLoS Pathog.* **6,** e1000782
16. Pietra, G., Romagnani, C., Falco, M., Vitale, M., Castriconi, R., Pende, D., Millo, E., Anfossi, S., Biassoni, R., Moretta, L., and Mingari, M. C. (2001) The analysis of the natural killer-like activity of human cytolytic T lymphocytes revealed HLA-E as a novel target for TCR α/β-mediated recognition. *Eur. J. Immunol.* **31,** 3687–3693
17. Pietra, G., Romagnani, C., Mazzarino, P., Falco, M., Millo, E., Moretta, A., Moretta, L., and Mingari, M. C. (2003) HLA-E-restricted recognition of cytomegalovirus-derived peptides by human CD8+ cytolytic T lymphocytes. *Proc. Natl. Acad. Sci. U.S.A.* **100,** 10896–10901
18. Hansen, S. G., Wu, H. L., Burwitz, B. J., Hughes, C. M., Hammond, K. B., Ventura, A. B., Reed, J. S., Gilbride, R. M., Ainslie, E., Morrow, D. W., Ford, J. C., Selseth, A. N., Pathak, R., Malouli, D., Legasse, A. W., *et al.* (2016) Broadly targeted $CD8^+$ T cell responses restricted by major histocompatibility complex E. *Science* **351,** 714–720
19. Tomasec, P., Braud, V. M., Rickards, C., Powell, M. B., McSharry, B. P., Gadola, S., Cerundolo, V., Borysiewicz, L. K., McMichael, A. J., and Wilkinson, G. W. (2000) Surface expression of HLA-E, an inhibitor of natural killer cells, enhanced by human cytomegalovirus gpUL40. *Science* **287,** 1031
20. Mazzarino, P., Pietra, G., Vacca, P., Falco, M., Colau, D., Coulie, P., Moretta, L., and Mingari, M. C. (2005) Identification of effector-memory CMV-specific T lymphocytes that kill CMV-infected target cells in an HLA-E-restricted fashion. *Eur. J. Immunol.* **35,** 3240–3247
21. Romagnani, C., Pietra, G., Falco, M., Mazzarino, P., Moretta, L., and Mingari, M. C. (2004) HLA-E-restricted recognition of human cytomegalovirus by a subset of cytolytic T lymphocytes. *Hum. Immunol.* **65,** 437–445
22. Hoare, H. L., Sullivan, L. C., Pietra, G., Clements, C. S., Lee, E. J., Ely, L. K., Beddoe, T., Falco, M., Kjer-Nielsen, L., Reid, H. H., McCluskey, J., Moretta, L., Rossjohn, J., and Brooks, A. G. (2006) Structural basis for a major histocompatibility complex class Ib-restricted T cell response. *Nat. Immunol.* **7,** 256–264
23. Gras, S., Wilmann, P. G., Chen, Z., Halim, H., Liu, Y. C., Kjer-Nielsen, L., Purcell, A. W., Burrows, S. R., McCluskey, J., and Rossjohn, J. (2012) A structural basis for varied $\alpha\beta$ TCR usage against an immunodominant EBV antigen restricted to a HLA-B8 molecule. *J. Immunol.* **188,** 311–321
24. Baker, B. M., Turner, R. V., Gagnon, S. J., Wiley, D. C., and Biddison, W. E. (2001) Identification of a crucial energetic footprint on the alpha1 helix of human histocompatibility leukocyte antigen (HLA)-A2 that provides functional interactions for recognition by tax peptide/HLA-A2-specific T cell receptors. *J. Exp. Med.* **193,** 551–562
25. Borg, N. A., Ely, L. K., Beddoe, T., Macdonald, W. A., Reid, H. H., Clements, C. S., Purcell, A. W., Kjer-Nielsen, L., Miles, J. J., Burrows, S. R., McCluskey, J., and Rossjohn, J. (2005) The CDR3 regions of an immunodominant T cell receptor dictate the 'energetic landscape' of peptide-MHC recognition. *Nat. Immunol.* **6,** 171–180
26. Burrows, S. R., Chen, Z., Archbold, J. K., Tynan, F. E., Beddoe, T., Kjer-Nielsen, L., Miles, J. J., Khanna, R., Moss, D. J., Liu, Y. C., Gras, S., Kostenko, L., Brennan, R. M., Clements, C. S., Brooks, A. G., *et al.* (2010) Hard wiring of T cell receptor specificity for the major histocompatibility complex is underpinned by TCR adaptability. *Proc. Natl. Acad. Sci. U.S.A.* **107,** 10608–10613
27. Godfrey, D. I., Rossjohn, J., and McCluskey, J. (2008) The fidelity, occasional promiscuity, and versatility of T cell receptor recognition. *Immunity* **28,** 304–314
28. Huseby, E. S., Crawford, F., White, J., Marrack, P., and Kappler, J. W. (2006) Interface-disrupting amino acids establish specificity between T cell receptors and complexes of major histocompatibility complex and peptide. *Nat. Immunol.* **7,** 1191–1199
29. Tynan, F. E., Burrows, S. R., Buckle, A. M., Clements, C. S., Borg, N. A., Miles, J. J., Beddoe, T., Whisstock, J. C., Wilce, M. C., Silins, S. L., Burrows, J. M., Kjer-Nielsen, L., Kostenko, L., Purcell, A. W., McCluskey, J., *et al.* (2005) T cell receptor recognition of a 'super-bulged' major histocompatibility complex class I-bound peptide. *Nat. Immunol.* **6,** 1114–1122
30. Joly, E., and Rouillon, V. (2006) The orthology of HLA-E and H2-Qa1 is hidden by their concerted evolution with other MHC class I molecules. *Biol. Direct* **1,** 2
31. Kulski, J. K., Gaudieri, S., and Dawkins, R. L. (2000) Using alu J elements as molecular clocks to trace the evolutionary relationships between duplicated HLA class I genomic segments. *J. Mol. Evol.* **50,** 510–519
32. Petrie, E. J., Clements, C. S., Lin, J., Sullivan, L. C., Johnson, D., Huyton, T., Heroux, A., Hoare, H. L., Beddoe, T., Reid, H. H., Wilce, M. C., Brooks, A. G., and Rossjohn, J. (2008) CD94-NKG2A recognition of human leukocyte antigen (HLA)-E bound to an HLA class I leader sequence. *J. Exp. Med.* **205,** 725–735
33. Sullivan, L. C., Clements, C. S., Beddoe, T., Johnson, D., Hoare, H. L., Lin, J., Huyton, T., Hopkins, E. J., Reid, H. H., Wilce, M. C., Kabat, J., Borrego, F., Coligan, J. E., Rossjohn, J., and Brooks, A. G. (2007) The heterodimeric assembly of the CD94-NKG2 receptor family and implications for human leukocyte antigen-E recognition. *Immunity* **27,** 900–911
34. Chang, L., Kjer-Nielsen, L., Flynn, S., Brooks, A. G., Mannering, S. I., Honeyman, M. C., Harrison, L. C., McCluskey, J., and Purcell, A. W. (2003) Novel strategy for identification of candidate cytotoxic T-cell epitopes from human preproinsulin. *Tissue Antigens* **62,** 408–417
35. Battye, T. G., Kontogiannis, L., Johnson, O., Powell, H. R., and Leslie, A. G. (2011) iMOSFLM: a new graphical interface for diffraction-image processing with MOSFLM. *Acta Crystallogr. D Biol. Crystallogr.* **67,** 271–281
36. Winn, M. D., Ballard, C. C., Cowtan, K. D., Dodson, E. J., Emsley, P., Evans, P. R., Keegan, R. M., Krissinel, E. B., Leslie, A. G., McCoy, A., McNicholas, S. J., Murshudov, G. N., Pannu, N. S., Potterton, E. A., Powell, H. R., *et al.* (2011) Overview of the CCP4 suite and current developments. *Acta Crystallogr. D Biol. Crystallogr.* **67,** 235–242
37. Kjer-Nielsen, L., Clements, C. S., Purcell, A. W., Brooks, A. G., Whisstock, J. C., Burrows, S. R., McCluskey, J., and Rossjohn, J. (2003) A structural basis for the selection of dominant $\alpha\beta$ T cell receptors in antiviral immunity. *Immunity* **18,** 53–64
38. Emsley, P., and Cowtan, K. (2004) Coot: model-building tools for molecular graphics. *Acta Crystallogr. D Biol. Crystallogr.* **60,** 2126–2132
39. Bricogne, G., Blanc, E., Brandl, M., Flensburg, C., Keller, P., Paciorek, W., Roversi, P., Sharff, A., Smart, O. S., Vonrhein, C., and Womack, T. O. (2016) *BUSTER*, Global Phasing Ltd., Cambridge, UK
40. Lefranc, M. P., Giudicelli, V., Kaas, Q., Duprat, E., Jabado-Michaloud, J., Scaviner, D., Ginestoux, C., Clément, O., Chaume, D., and Lefranc, G. (2005) IMGT, the international ImMunoGeneTics information system. *Nucleic Acids Res.* **33,** D593–D597
41. DeLano, W. L. (2015) *The PyMOL Molecular Graphics System*, Version 1.8, Schrödinger, LLC, New York

A conserved energetic footprint underpins recognition of human leukocyte antigen-E by two distinct αβ T cell receptors

Lucy C. Sullivan, Nicholas G. Walpole, Carine Farenc, Gabriella Pietra, Matthew J. W. Sum, Craig S. Clements, Eleanor J. Lee, Travis Beddoe, Michela Falco, Maria Cristina Mingari, Lorenzo Moretta, Stephanie Gras, Jamie Rossjohn and Andrew G. Brooks

J. Biol. Chem. 2017, 292:21149-21158.
doi: 10.1074/jbc.M117.807719 originally published online September 25, 2017